ELSEVIER

Chemical Engineering Journal 85 (2002) 17–25

Chemical Engineering Journal

www.elsevier.com/locate/cej

On the effect of tracer density on axial dispersion in a batch oscillatory baffled column

Xiongwei Ni [a,*], Yann Sommer de Gélicourt [a], John Neil [a], Tony Howes [b]

[a] *Department of Mechanical and Chemical Engineering, Heriot-Watt University, Edinburgh, Scotland EH14 4AS, UK*
[b] *Department of Chemical Engineering, University of Queensland, St. Lucia 4072, Australia*

Received 23 September 2000; received in revised form 22 January 2001; accepted 22 January 2001

Abstract

In this paper, we report our modelling evaluation on the effect of tracer density on axial dispersion in a batch oscillatory baffled column (OBC). Tracer solution of potassium nitrite, its specific density ranged from 1.0 to 1.5, was used in the study, and was injected to the vertical column from either the top or bottom. Local concentration profiles are measured using conductivity probes at two locations along the height of the column. Using the experimental measured concentration profiles together with both 'Tank-in-Series' and 'Plug Flow with Axial Dispersion' models, axial dispersion coefficients were determined and used to describe the effect of specific tracer density on mixing in the OBC. The results showed that the axial dispersion coefficients evaluated by the two models are very similar in both magnitudes and trends, and the range of variations in such coefficients is generally larger for the bottom injection than for the top one. Empirical correlations linking the mechanical energy for mixing, the specific density of tracer and axial dispersion coefficient were established. Using these correlations, we identified the enhancements of up to 269% on axial dispersion for various specific tracer densities.

Keywords: Axial dispersion coefficient; Oscillatory baffled column; Tracer density; Tanks-in-series model; Plug flow with axial dispersion model

1. Introduction

Batch reactors have widely been employed by polymer manufacturers. Taking suspension polymerisation process as an example, a continuous aqueous phase, usually water, is contained and agitated in a batch vessel while a water-insoluble monomer is charged, dispersed and suspended as droplets in the aqueous phase. Polymerisation is initiated by a monomer-soluble initiator, and polymer particles (beads) occur within the monomer droplets. The density of monomer/initiator over the continuous phase can be different depending on the specific type of polymer to be made, from a relative density difference $\Delta\rho/\rho$ of $\sim$0.05 for methylmethacrylate to $\Delta\rho/\rho$ of from 1.08 to 1.3 for acrylamide for example. It has been observed that the charge of denser monomer often brings about variations on droplet and subsequent final particle size distribution [1,2], and this is believed due to the enhanced axial dispersion occurred in batch vessels. The objective of this work is to study the effect of density variation on the underlying dispersion in a batch oscillatory baffled column (OBC).

The OBC is a relatively new mixing device in which fluid mixing is achieved by eddies that are generated when fluid passes through a set of equally spaced stationary orifice baffles. Those periodically formed vortices can be controlled by a combination of geometrical and operational parameters, such as, baffle diameter, baffle spacing, oscillation frequency and amplitude. Under certain operational conditions, the OBC can be operated as either a plug flow reactor or an enhanced mixing device [3–7]. For a given baffle geometry, the fluid mechanical condition in an OBC is controlled by the oscillatory Reynolds number, Re_o, and the Strouhal number, St, defined as

$$Re_o = \frac{\rho D x_o \omega}{\mu} \tag{1}$$

$$St = \frac{D}{4\pi x_o} \tag{2}$$

where D is the column diameter (m), x_o the oscillation amplitude (m), ω the angular frequency of oscillation ($=2\pi f$), f the oscillation frequency (Hz), μ the dynamic viscosity of fluid (Ns m^{-2}) and ρ the density of the liquid (kg m^{-3}). The

* Corresponding author. Tel.: +44-131-451-3781; fax: +44-131-451-3077.
E-mail address: x.ni@hw.ac.uk (X. Ni).

1385-8947/02/$ – see front matter
PII: S1385-8947(01)00137-1

Nomenclature

C	concentration of species ($g\,dm^{-3}$)
C_D	orifice discharge coefficient (=0.7)
C_0	initial concentration ($g\,dm^{-3}$)
D	tube diameter (m)
D_0	baffle hole diameter (m)
E	axial dispersion coefficient ($cm^2\,s^{-1}$)
f	oscillation frequency (Hz)
H	dimensionless baffle spacing
L	vessel length (m)
M	constant
N	constant
N_B	number of baffles per unit length (m^{-1})
P/V	power density ($W\,m^{-3}$)
Q	inter-cell mixing flowrate ($m^3\,s^{-1}$)
Re_o	oscillatory Reynolds number defined by Eq. (1)
St	Strouhal number defined by Eq. (2)
t	time variable (s)
V_{cell}	inter-baffle cell volume (m^3)
x_o	amplitude of oscillation (m)
Z	distance at axial direction (m)

Greek symbols

α	ratio of baffle open area to tube area
ε	power input per mass ($W\,kg^{-1}$)
λ	constant
μ	dynamic viscosity of fluid ($Ns\,m^{-2}$)
ρ	density of fluid ($kg\,m^{-3}$)
τ_{mix}	cell residence time (s)
ω	angular frequency of oscillation (radians s^{-1})
Φ	dimensionless axial dispersion

Subscripts

B	injection from bottom port
T	injection from top port
ts	the 'Tanks-in-Series' model
pfad	the 'Plug Flow with Axial Dispersion' model

power density of an OBC can be estimated from [8]

$$\frac{P}{V} = \frac{2\rho N_B}{3\pi C_D^2}\frac{1-\alpha^2}{\alpha^2}x_o^3\omega^3 \quad (3)$$

where N_B is the number of baffles per unit length (m^{-1}), α the baffle free area ratio ($=(D_0/D)^2$) where D_0 is the orifice diameter (m) and C_D the orifice discharge coefficient (taken as 0.7). For a given baffle geometry, the power input in an OBC is proportional to the cube of the oscillatory velocity, $x_o f$.

Research into axial dispersion in oscillatory-baffled flow has so far been centred on using neutrally buoyant tracer solutions [5–7,9,10]. In recent applications of oscillatory-baffled reactors to polymerisation processes [11], the effect of tracer density on droplet size distribution has become evident. This current study aims at investigating of such an effect on axial dispersion.

2. Materials and methods

2.1. The oscillatory-baffled column

A schematic diagram of the experimental apparatus and facilities is given in Fig. 1. The OBC consists of a vertical Perspex column of 50 mm in diameter and 950 mm in height. The liquid height used in our experiments was 865 mm, making a test volume of 1.7 dm^3. A stainless steel piston was used to generate fluid oscillation at the base of the OBC. It was driven by a cam actuated by an electrical motor and a gear box. The speed of the motor was controlled to provide oscillation frequencies from 1 to 10 Hz. The oscillation amplitudes of 1–15 mm centre-to-peak can be obtained by adjusting the off-centre positions of the connecting pin in a flying wheel. Two oscillation amplitudes of 3 and 6.5 mm and three oscillation frequencies of 2, 3 and 4 Hz were used in the experiments, and the corresponding oscillatory Reynolds numbers ranged from 1884 to 12,252.

Baffles, made of polyethylene plates, were used in the experiments and supported by two 3 mm diameter stainless steel rods. The baffles were spaced equally at 75 mm apart and fitted close to the wall. The baffle hole diameter was 23 mm, making the ratio of baffle open area to tube area of 21%.

Two Vernier conductivity probes were used to monitor the changes of concentration of potassium nitrite (KNO_2) against time along the height of the column. The probes are automatically temperature-compensated between 5 and 35 °C. Prior to the start of the experiments, the conductivity

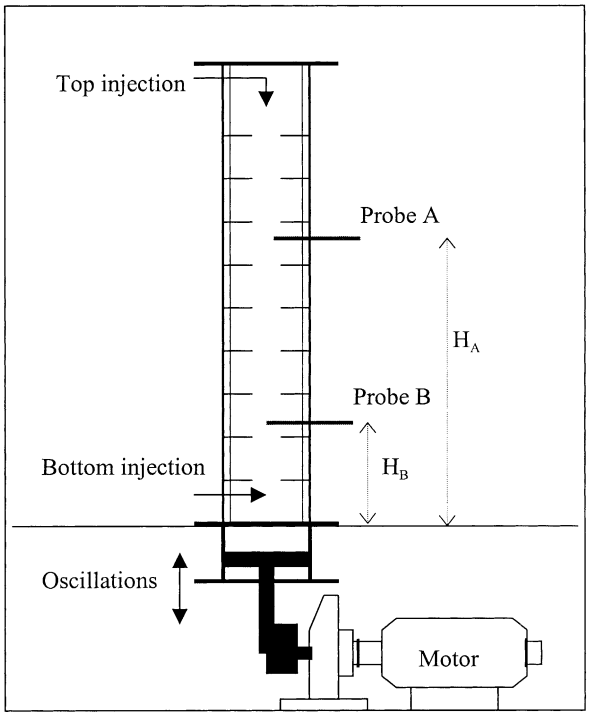

Fig. 1. Schematic diagram of the OBC ($H_A = 570$ mm, $H_B = 195$ mm).

probes were calibrated using the standard two-point method at 0 mg dm^{-3} (using deionised water) and 500 mg dm^{-3} concentration of KNO_2. The probes, of 10 mm diameter and 100 mm long, were placed so that the tips of the probes are located in the centre of the column. The sensors were connected to a multi purpose lab interface (MPLI) and the signals are shown in real-time graphic mode as well as in a tabulated form. The rate of data gathering for both probes was set at three readings per second, and the upper probe was labelled A and the lower probe B. The experimental duration ranged from 300 to 900 s.

In this study, potassium nitrite, instead of the more commonly used sodium chloride, was used as the tracer since it has a much greater solubility at room temperature than sodium chloride, thus giving wider variation of tracer density. The tracer *solution* can be injected from either the top or the bottom port. The tracer concentrations ranged from 233 to 2265 g_{KNO_2} per litre of water, giving the specific density range of the tracer solution from 1.1 to 1.5.

2.2. Experimental procedure

The experiments started by applying oscillation to the OBC filled with water at a pre-set oscillation amplitude and frequency, and then initiating the data capture via the MPLI program. After an arbitrary delay of 10 s, a known amount of KNO_2 tracer of a given specific density was injected via either the top or bottom port, typically 4 ml for the top injection and 6 ml for the bottom injection due to the port construction where an estimated 2 ml of tracer was contained by the injection channel itself. Data recorded in this way contains both the pre and in situ events of concentration versus time in the column. The MPLI program stopped automatically when the duration of the pre-set experimental time was reached. The column was then drained and washed with water before a new experiment was initiated. A total of 136 experiments were carried out, covering all the pre-described parameters and conditions. In addition, around about 10% of the experiments were repeated for consistency and repeatability.

2.3. Concentration profiles

The changes of tracer concentrations are measured as a function of time, and plotted in Figs. 2 and 3 for a specific tracer density of 1.1. It can be seen that the change of concentrations instantly felt by the top probe for the top injection (Fig. 2). The change registered by the bottom probe was smaller and slightly later than that by the top probe. Both concentration curves quickly converged to an equilibrium concentration. For the bottom injection (Fig. 3), a similar profile but with a reverse order is observed compared to that showed in Fig. 2. In this case, it was the bottom probe that responded first for the bottom injection, and the top probe that followed. Using the same formula and optimisation

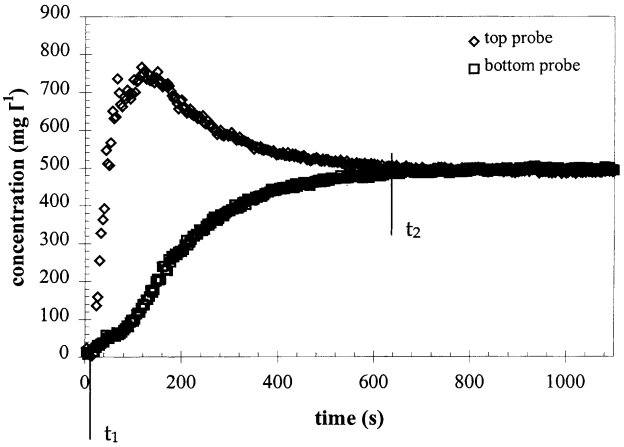

Fig. 2. Concentration vs. time. Oscillation frequency = 2 Hz. Oscillation amplitude = 3 mm. Tracer specific density = 1.1. Injection location = top.

procedure described elsewhere [12], the mixing time ($t_2 - t_1$) can be estimated from the concentration profiles, and tabulated in Table 1. It can be seen that at any given specific density, the mixing time at the bottom injection was larger than that at the top for the ranges of oscillatory Reynolds numbers tested. The extent of this decreased with the increase of the specific density of the tracer, indicating that the tracer density did have an effect on the characteristics of mixing in the OBC. The effect of tracer density was most noticeable for low oscillatory Reynolds numbers. The observed reduction of mixing time was 68% for the lowest Reynolds number but only 17% for the highest one, when the tracer density was changed from 1.0 to 1.5.

Axial dispersion is recognised as a universal measure of mixing characteristics in chemical reactors. In the following sections, we establish the effect and relationship of tracer density as such the axial dispersion coefficient.

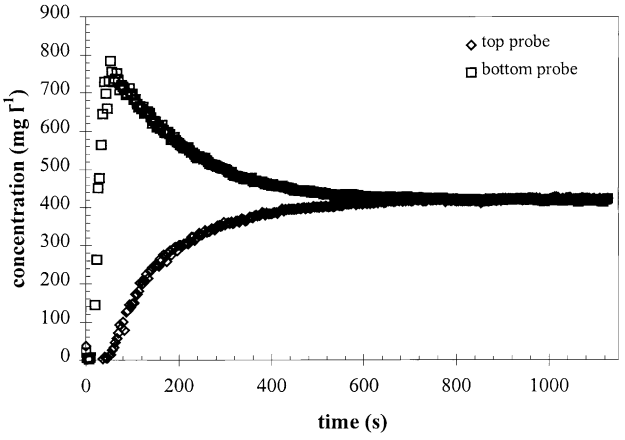

Fig. 3. Concentration vs. time. Oscillation frequency = 2 Hz. Oscillation amplitude = 3 mm. Tracer specific density = 1.1. Injection location = bottom.

Table 1
Mixing times evaluated for both top and bottom tracer injections

S_p	$x_o f$ (cm s^{-1})	Re_o	Bottom injection		Top injection	
			Q (cm^3 s^{-1})	τ_{mix} (s)	Q (cm^3 s^{-1})	τ_{mix} (s)
1.0	0.6	1885	6	24	3	45
	1.95	6126	23	6	36	4
	2.6	8168	49	3	63	2
1.1	0.6	2073	9	16	7	22
	1.95	6739	31	5	29	5
	2.6	8985	47	3	45	3
1.2	0.6	2262	11	14	8	19
	1.95	7351	41	4	33	5
	2.6	9802	69	2	51	3
1.3	0.6	2450	23	7	15	10
	1.95	7964	54	3	31	5
	2.6	10619	71	2	56	3
1.4	0.6	2639	19	8	14	10
	1.95	8577	50	3	30	5
	2.6	11435	72	2	56	3
1.5	0.6	2827	20	7	15	10
	1.95	9189	49	3	32	5
	2.6	12252	67	2	55	3

Table 2
Inter-cell mixing flowrates and cell residence times

S_p	$x_o f$ (cm s^{-1})	Re_o	Mixing time (s)	
			Bottom injection	Top injection
1.0	0.6	1885	919	888
	1.95	6126	247	106
	2.6	8168	115	102
1.1	0.6	2073	606	586
	1.95	6739	233	155
	2.6	8985	152	99
1.2	0.6	2262	477	475
	1.95	7351	142	120
	2.6	9802	177	91
1.3	0.6	2450	245	244
	1.95	7964	129	108
	2.6	10619	94	84
1.4	0.6	2639	287	282
	1.95	8577	129	115
	2.6	11435	90	84
1.5	0.6	2827	290	272
	1.95	9189	122	117
	2.6	12252	95	84

3. Axial dispersion

Two models, 'Tanks-in-Series' and 'Plug Flow with Axial Dispersion', have been used for the determination of axial dispersion coefficients in our batch OBC.

3.1. Tanks-in-series model

Howes [13] applied the 'Tank-in-Series' model to determine axial dispersion in an oscillatory baffled tube. In this method, the tube was modelled as a series of perfect stirred tanks with each tank representing an inter-baffle cell, where there is an inter cell mixing flowrate, Q. The tanks have been labelled such that the cell number nearer to the tracer injection is zero. Denoting that C_n is the concentration measured by a probe in the cell nearer to the injection point and C_f the concentration measured by a probe in the cell further away from injection. Using the imperfect tracer pulse method and set values for Q and C_n, the concentrations in all the other tanks can be calculated by solving the following difference equation based on a numerical approach from [14]:

$$t = 0, \quad C_0(0) = C_n(0) \tag{4}$$

$$C_p(0) = 0 \quad 1 \le p \le M \tag{5}$$

$$C_0(t + \Delta t) = C_n(t + \Delta t) \tag{6}$$

$$C_p(t + \Delta t) = C_p(t) + \frac{\Delta t Q}{V_{cell}}[C_{p-1}(t) + C_{p+1}(t) - 2C_p(t)], \quad 1 \le p \le M \tag{7}$$

$$C_M(t + \Delta t) = C_M(t) + \frac{\Delta t Q}{V_{cell}}\left[C_{M-1}(t) - C_M(t)\right] \tag{8}$$

where M is the number of baffle cells after the first probe in relation to the tracer injection (=6 for the bottom injection, 5 for the top) and N the numbers of inter-baffle cells between the two probes (=3 for both injection ports). The calculated concentration, C_{N+1}, is then compared with the experimental one, C_f, until $\sum_{t=0}^{t_\infty}[C_{N+1}(t) - C_f(t)]^2$ is minimised, and in this way Q can be determined. From this, a cell residence time, τ_{mix} (=V_{cell}/Q), and a dimensionless axial dispersion number, Φ, defined below are calculated [12]:

$$\Phi = \frac{\rho E_{ts}}{\mu} = \frac{H^2 Re_o St}{2\tau_{mix} f} \tag{9}$$

where H is the dimensionless baffle spacing and E_{ts} the axial dispersion coefficient evaluated using the Tanks-in-Series model (cm^2 s^{-1}). Table 2 shows the evaluated inter-cell mixing flowrates and cell residence times for various oscillation conditions and for six specific tracer densities. The longer the cell residence time, the less the mixing. It can be seen from Table 2 that at any given specific tracer density τ_{mix} decreases with the increase of oscillatory velocity. This agrees with our expectation. By comparing the cell residence times between the smallest and largest specific tracer densities, the results are that τ_{mix} is smaller for the latter than for the former, indicating the effect of tracer density on cell residence time. It should be noted that such differences decrease significantly with the increase of oscillation intensities. At the highest oscillatory velocity of 2.6 cm s^{-1}, there is very little difference in τ_{mix} between various tracer densities.

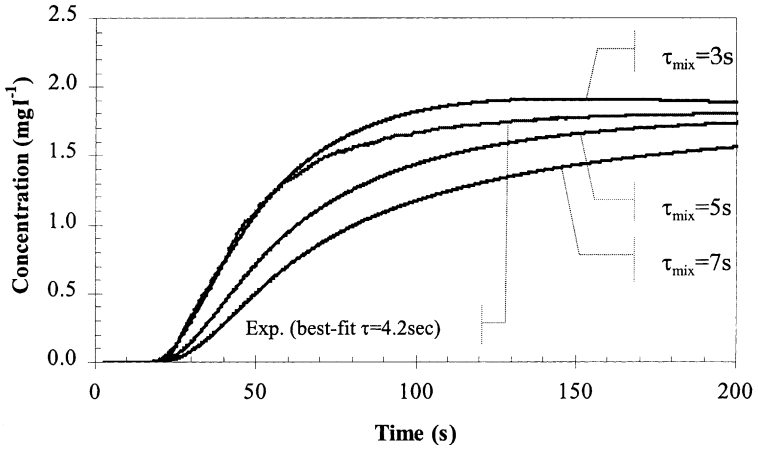

Fig. 4. Calculated and experimental concentration. Injection location: bottom. Density = 1.5. Oscillatory frequency = 2 Hz. Oscillatory amplitude = 6.5 mm.

Fig. 4 plots the measured values of C_f alongside the calculated values of C_{N+1}, given $\tau_{mix} = 3, 5$ and 7 s. The oscillation frequency was 2 Hz, the centre-to-peak amplitude was 6.5 mm and the tracer specific density was 1.5. The best-fit value for τ_{mix} was found to be equal to 4.32 s. The close similarity between the experimental and calculated concentration profiles validates the model.

Figs. 5 and 6 plot the axial dispersion coefficients calculated from the 'Tank-in-series' model with respect to the oscillatory velocity for all the six specific tracer densities at the top and bottom tracer injection, respectively. It is clear from the two figures that the axial dispersion coefficients increased with the increase of the oscillatory velocity, i.e. oscillation intensity, for all specific densities tested. At a given oscillatory velocity, the higher the tracer specific density, the more the axial dispersion for both injections. Generally, there is not much difference in the magnitudes of axial dispersion coefficients between top and bottom injections, although the range of variation in the coefficient is larger for the bottom port than for the top.

3.2. 'Plug flow with axial dispersion' model

In a manner analogous to Fick's law of molecular diffusion [15], the contributions due to eddy mixing in OBC can be described by a quantitative parameter, E, the axial dispersion coefficient. The governing equation for a batch reactor of length L is

$$\frac{\partial C}{\partial t} = E\frac{\partial^2 C}{\partial Z^2} \tag{10}$$

where C is the concentration (g dm^{-3}), t the time (s) and Z the axial direction (m). An exact analytical solution of the partial differential equations is difficult to obtain, however,

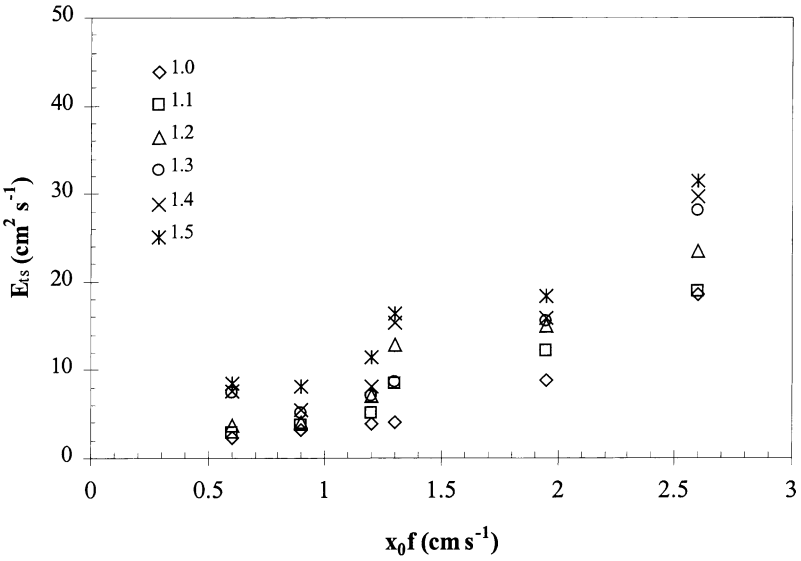

Fig. 5. Axial dispersion coefficient vs. oscillatory velocity. Injection location: TOP 'Tanks-in-series' model.

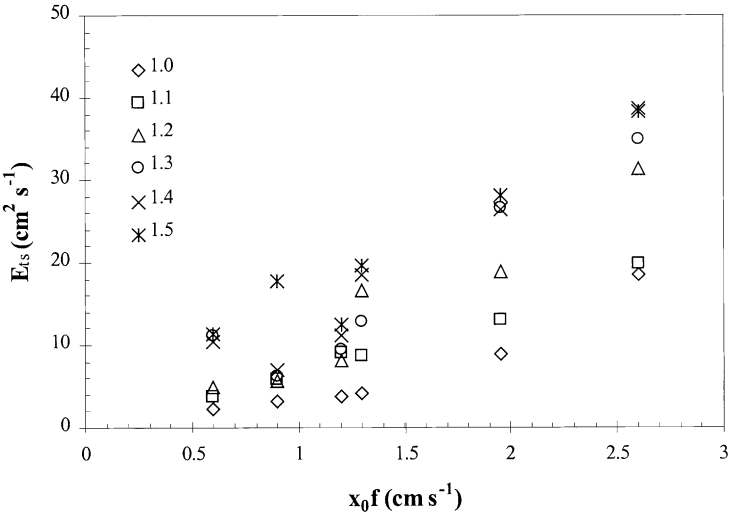

Fig. 6. Axial dispersion coefficient vs. oscillatory velocity. Injection location: BOTTOM 'Tanks-in-series' model.

numerical results are widely used. For pulse injection of a tracer, the concentration profile at time t is given by

$$C = C_0 \left\{ 1 + 2\sum_{n=1}^{\infty} \exp\left[-Et \left(\frac{n\pi}{L} \right)^2 \right] \cos\left(\frac{n\pi Z}{L} \right) \right\} \quad (11)$$

where C_0 is the initial concentration (g dm^{-3}). For large values of t, the non-ideal pulse is less important and only the first term ($n = 1$) in the series is significant, thus, Eq. (11) can be simplified as

$$C \approx C_0 \left[1 + 2 \exp\left(\frac{-E\pi^2 t}{L^2} \right) \cos\left(\frac{\pi Z}{L} \right) \right] \quad (12)$$

Measuring C_1 at Z_1, i.e. the probe location A and C_2 at Z_2, the location B, we have

$$C_1 - C_2 = 2C_0 \exp\left(\frac{-E\pi^2 t}{L^2} \right) \times \left[\cos\left(\frac{\pi Z_1}{L} \right) - \cos\left(\frac{\pi Z_2}{L} \right) \right] \quad (13)$$

and

$$\ln(C_1 - C_2) = -\frac{E\pi^2}{L^2} t + \text{const.} \quad (14)$$

By plotting $\ln(C_1 - C_2)$ versus t, we can estimate E from the slope, i.e.

$$-\frac{E_{\text{pfad}}\pi^2}{L^2} = \text{averaged slope} \quad (15)$$

As a result, E_{pfad} can finally be calculated from Eq. (15), where the subscripts of pfad stand for Plug Flow with Axial Dispersion model.

Figs. 7 and 8 show the axial dispersion coefficients calculated using the 'Plug Flow with Axial Dispersion' model against the oscillatory velocity at both injection locations. It is again clear that the axial dispersion coefficients increase with the increase of oscillation intensity for both injection ports. The range of variations in magnitude is also larger for the bottom port than for the top one. In comparison to these shown in Figs. 5 and 6, it is easy to see that the magnitudes and trends in axial dispersion coefficients evaluated by the two models are closely matched. This indicates the validity of both the 'Plug Flow with Axial Dispersion' and the 'Tanks-in-series' model for describing the mixing characteristics in batch OBCs. In the following sections of the paper, the axial dispersion coefficients from the 'Tanks-in-Series' model were used as it has much less simplification procedures during evaluation, and gives more information on mixing, e.g. E_{ts}, Q, t_{mix}. Figs. 9 and 10 plot the axial dispersion coefficients for both top and bottom injections as a function of oscillatory Reynolds numbers. The best-fits to the axial dispersion coefficient data give:

$$(E_{\text{ts}})_{\text{TOP}} = 1.89 Re_{\text{o}}^{1.26} \quad (16)$$

$$(E_{\text{ts}})_{\text{BOTTOM}} = 2.43 Re_{\text{o}}^{1.26} \quad (17)$$

It is interesting to notice that the axial dispersion coefficients share the same power index on the oscillatory Reynolds number for both top and bottom injections. This is expected as the same oscillatory conditions and identical tracer solution were applied to the column. The best-fit constant is, however, slightly larger for the bottom injection than for the top one, and this gives about 29% higher in axial dispersion for a given tracer density. The results presented here seem counter-intuitive. The expectation is that the high density of tracer would cause more dispersion when injected from the top, while suppress dispersion when injected from the bottom. The possible reason for this could be due to the secondary dispersion generated when tracer solution entered from the bottom of the column. In this case, each element of tracer is in motion with fluid oscillation, up and down the column. When these elements are elevated, it produces the secondary dispersion on the downward flow. Such an effect

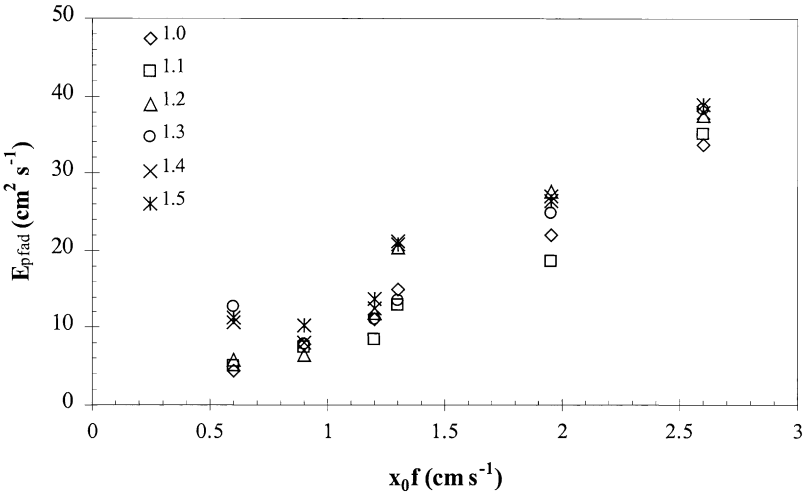

Fig. 7. Axial dispersion coefficient vs. oscillatory velocity. Injection location: TOP. 'Axial dispersion' model.

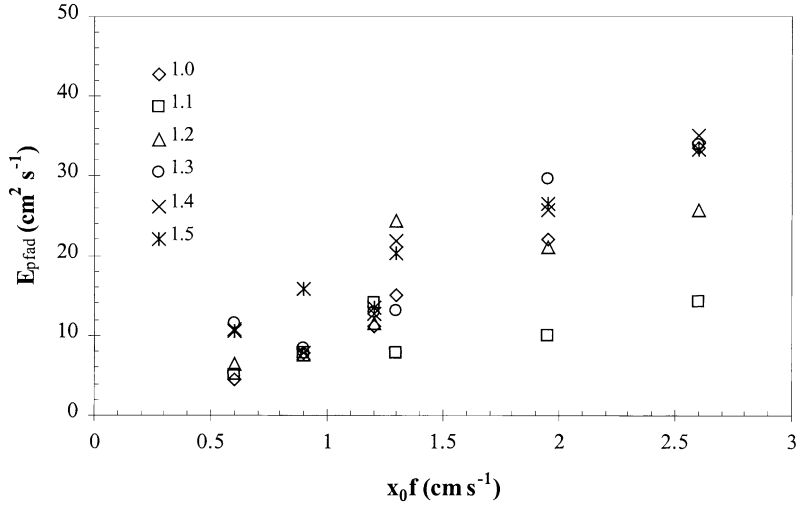

Fig. 8. Axial dispersion coefficient vs. oscillatory velocity. Injection location: BOTTOM 'Axial dispersion' model.

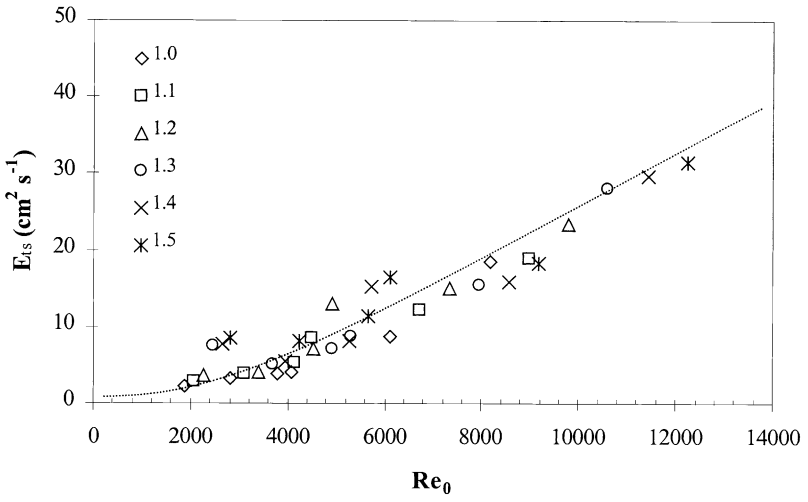

Fig. 9. Axial dispersion coefficient vs. oscillatory Reynolds number. Injection location: TOP. 'Tanks-in-series' model.

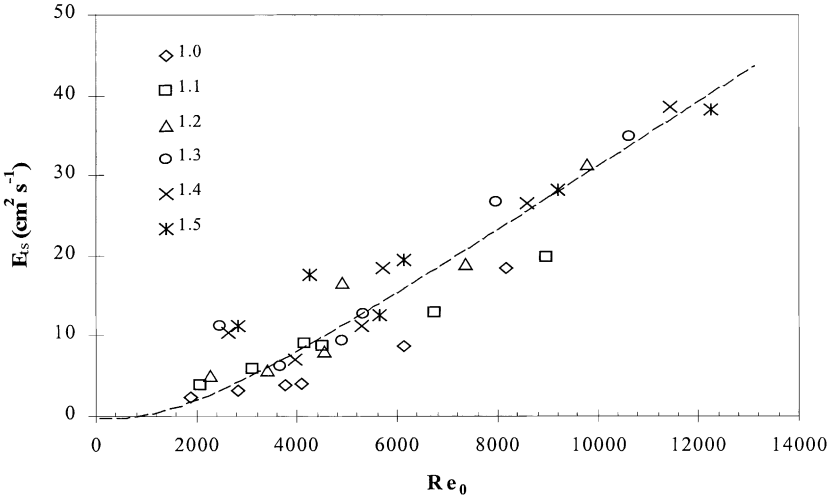

Fig. 10. Axial dispersion coefficient vs. oscillatory Reynolds number. Injection location: BOTTOM. 'Tanks-in-series' model.

would be more pronounced at the lower parts of the column than at the upper regions, because only the elements with lesser density could be pushed to the top of the column. For the top injection, the potential 'energy' for these tracer elements to go down is much greater, and subsequently the effect of oscillation on this is less sensitive as compared to the case of bottom injection.

3.3. Evaluation of gravity added axial dispersion

In order to quantify the axial dispersion induced by the density difference, we assume that axial dispersion has a power law relationship with the tracer density and mechanical energy for mixing as

$$E = E_{1.0} + \lambda \left(\frac{\Delta\rho}{\rho}\right)^m \varepsilon^n \tag{18}$$

where $E_{1.0}$ is the axial dispersion obtained for neutrally buoyant tracers (cm^2 s^{-1}), λ a dimensional constant, $\Delta\rho/\rho$ the relative density difference between the tracer solution and bulk fluid per unit density of the bulk, and ε the mechanical energy dissipation (W kg^{-1}) of an OBC ($\varepsilon = P/\rho V$). From non-linear curve fitting, the best-fit coefficients λ, m and n are obtained for both the top and bottom injections

$$(E_{ts})_{TOP} = E_{1.0} + 45.1 \left(\frac{\Delta\rho}{\rho}\right)^{0.521} \varepsilon^{0.251} \tag{19}$$

$$(E_{ts})_{BOTTOM} = E_{1.0} + 49.7 \left(\frac{\Delta\rho}{\rho}\right)^{0.787} \varepsilon^{0.251} \tag{20}$$

Similar features can be extracted from these two equations as compared with those shown in Figs. 9 and 10. Firstly, the indexes for the power dissipation are the same for axial dispersion coefficients at the two injection locations; this is expected, as the mechanical power input did not change during the experiments. Secondly, it can be seen that the index of the tracer density for E_{BOTTOM} is greater than that for E_{TOP}. This highlights the fact that the tracer density has more influence on axial dispersion when the tracer is injected via the bottom port rather than the top port. The

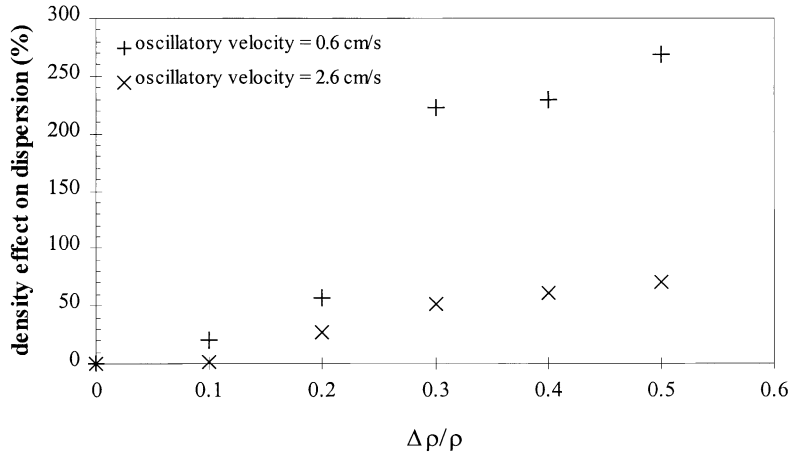

Fig. 11. Effect of relative density difference on dispersion.

exact percentage of the effect of added density on dispersion can be quantified by defining:

$$\%\text{effect} = \frac{E - E_{1.0}}{E_{1.0}} \quad (21)$$

Fig. 11 illustrated that the percentage of effect for two oscillatory velocities of 0.6 and 2.6 cm s^{-1}, respectively. We can see that the percentage increases with the density as expected but seems to level off for high densities. With the increase of oscillatory intensity, such percentages of effect on dispersion become less sensitive. In summary, this effect was found to vary from 2% for the smallest specific tracer density to 269% for the largest.

4. Conclusions

We have reported our model evaluations on the influence of tracer density on axial dispersion in a batch 50 mm diameter OBC. The tracer concentrations ranged from 43 to 2265 g_{KNO_2} per litre of water, giving the specific density of the tracer solution from 1.0 to 1.5. It was found that at any given oscillatory velocity, the more the tracer density, the more the axial dispersion. The percentage of the effect varies from 2 to 269%. This means that such percentages of axial dispersion should be added to $E_{1.0}$ when the specific tracer density increases from 1.0 to 1.5.

Acknowledgements

The authors wish to thank the ERASMUS for financial support of Mr Yann Sommer de Gélicourt.

References

[1] X. Ni, Y. Zhang, I. Mustafa, An investigation of droplet size and size distribution in methyl methacrylate suspensions in a batch oscillatory baffled reactor, Chem. Eng. Sci. 53 (1998) 2903–2919.
[2] X. Ni, Y. Zhang, I. Mustafa, Correlation of polymer particle size with droplet size in suspension polymerization of methyl methacrylate in a batch oscillatory baffled reactor, Chem. Eng. Sci. 5–54 (1999) 841–850.
[3] C.R. Brunold, J.C.B. Hunns, M.R. Mackley, Thompson, experimental observations on flow patterns and energy losses for oscillatory flows in ducts with sharp edges, Chem. Eng. Sci. 44 (1989) 1227–1244.
[4] A.W. Dickens, M.R. Mackley, H.R. Williams, Experimental residence time distribution measurements for unsteady flow in baffled tubes, Chem. Eng. Sci. 44 (1989) 1471–1479.
[5] T. Howes, M.R. Mackley, Experimental axial dispersion for oscillatory flow through a baffled tube, Chem. Eng. Sci. 45 (1990) 1349–1358.
[6] M.R. Mackley, X. Ni, Mixing and dispersion in a baffled tube for steady laminar and pulsative flow, Chem. Eng. Sci. 46 (1991) 3139–3151.
[7] M.R. Mackley, X. Ni, Experimental fluid dispersion measurements in periodic baffled tube arrays, Chem. Eng. Sci. 48 (1993) 3293–3305.
[8] M.H.I. Baird, P. Stonestreet, Energy dissipation in oscillatory flow within a baffled tube, Chem. Eng. Res. Design 73 (1995) 503–511.
[9] T. Howes, M.R. Mackley, E.P.L. Roberts, The simulation of chaotic mixing and dispersion for periodic flows in baffled channels, Chem. Eng. Sci. 46 (1991) 1669–1677.
[10] X. Ni, A study of fluid dispersion in oscillatory flow through a baffled tube, J. chem. Technol. Biotechnol. 64 (1995) 165–174.
[11] X. Ni, G. Nelson, I. Mustafa, Flow patterns and oil-water dispersion in a 0.38 m diameter oscillatory baffled column, Can. J. Chem. Eng. 78 (1) (2000) 211–220.
[12] N. Harnby, M.F. Edwards, A.W. Nienow, Mixing in the Process Industries, 2nd Edition, Butterworths, UK, 1992.
[13] T. Howes, On the Dispersion of Unsteady Flow in Baffled Tubes, Ph.D. Thesis, Cambridge University, Cambridge, 1988.
[14] J.C. Mecklenburgh, S. Hartland, The Theory of Backmixing, Wiley, UK, 1975.
[15] E.L. Cussler, Diffusion, Mass Transfer in Fluid Systems, Cambridge University Press, Cambridge, 1984.